Supporting Information

Synergistic Coupling of Photo and Thermal Conditions for Enhancing CO_2 Reduction Rates in the Reverse Water Gas Shift Reaction.

Joel Y.Y Loh[a], Yufeng Ye[b], Nazir P. Kherani[a,c]*

[a] Electrical and Computing Engineering, University of Toronto, Toronto, Ontario M5S 3G4, Canada.

[b] Research Laboratory of Electronics, Massachusetts Institute of Technology, 50 Vassar St, Cambridge, MA 02142, USA

[c] Material Science and Engineering, University of Toronto, Toronto, Ontario M5S 3E4, Canada.

Corresponding author: kherani@ecf.utoronto.ca *

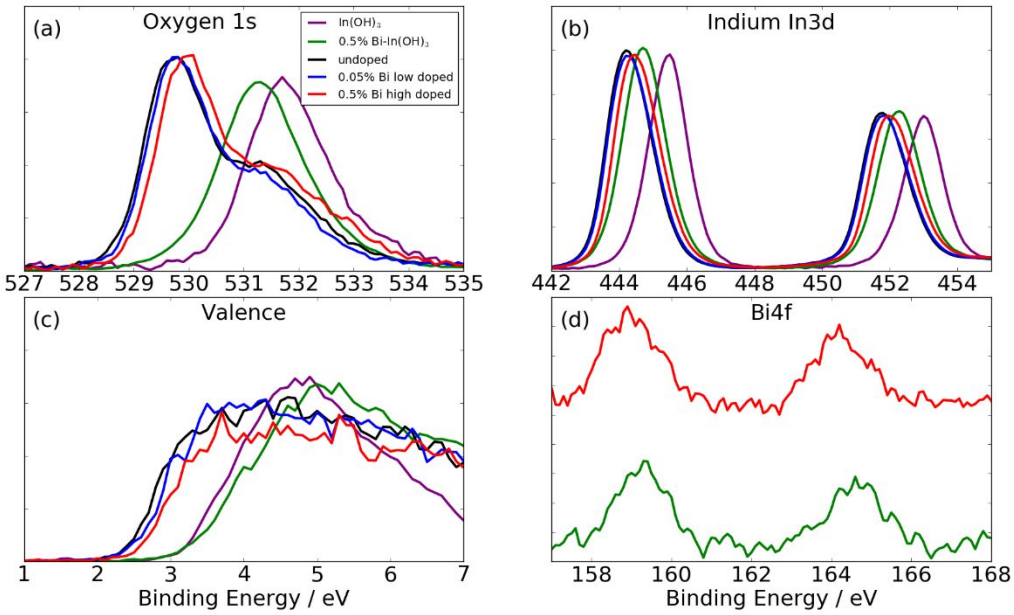

Figure S1. The XPS spectra of (a) O1s (b) In3d, valence band edge (c) and Bi4f (d), of $In(OH)_3$ (purple), 0.5% bismuth doped Bi-$In(OH)_3$, undoped $In_2O_{3-x}OH_y$ (black), low doped 0.05% a.t $Bi_zIn_{2-z}O_{3-x}OH_y$ (blue), and high doped 0.5% a.t $Bi_zIn_{2-z}O_{3-x}OH_y$ (red).

The XPS spectra of the indium hydroxide precursor and doped indium hydroxide precursor, where bismuth doping actually decreases the binding energy of the hydroxide due to the increased negative charge injection into the lattice structure surrounding the hydroxide. To be specific, the higher electronegativity of Bi(III) compared to In(III) cannot account for the shift to low energy. Instead, the 6s2 lone pair of electrons that exists for Group V Bi(III) and not for Group III In(III) most likely accounts for the enhanced electron density on the OH group of $Bi_zIn_{1-z}(OH)_3$ compared to $In(OH)_3$. The lower binding energy of O1s in bismuth doped $In(OH)_3$ indicates that H^+ is not as strongly bound to the O as that of In(OH)3 which indicates lower hygroscopicity of bismuth doped $In(OH)_3$. Furthermore, a small amount of bismuth doping of indium shifts the indium 3d peak close to an indium oxide value. In all, these results show that bismuth doped $In(OH)_3$ likely dehydrolyzes towards the In_2O_3 phase more readily than undoped $In(OH)_3$ which also supports the notion that Bi–OH terminated species is less likely than In-OH species.

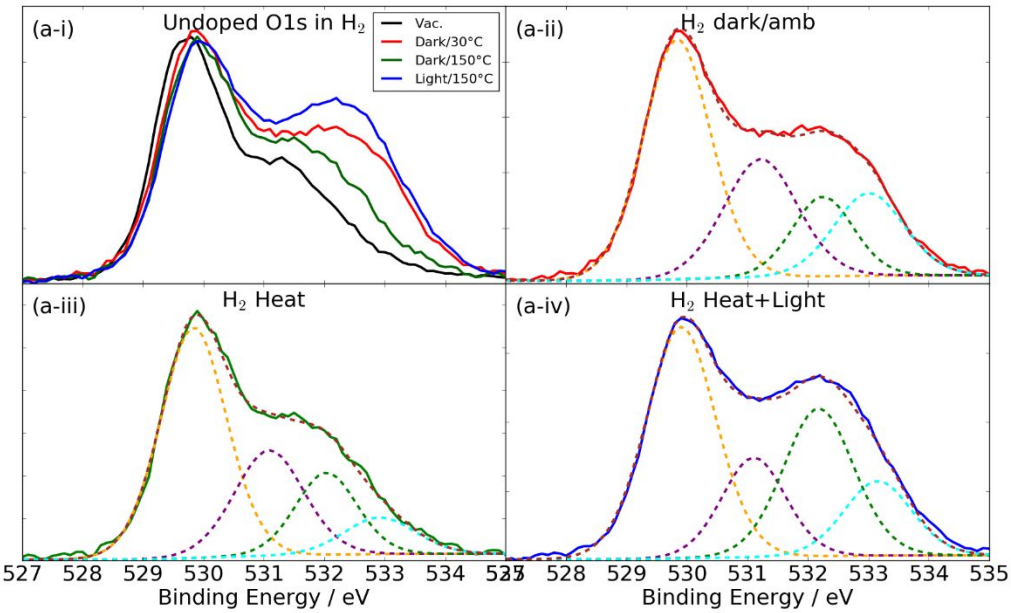

Figure S2. The O1s of the undoped sample in H_2 post the various reactor conditions and the deconvolution. (a-i) shows all the various reactor conditions. (a-ii) shows the O1s spectrum in H_2 dark ambient temperature. (a-iii) shows the O1s spectrum in H_2 dark 150°C. (a-iv) shows the O1s spectrum in H_2 photo-illumination 150°C.

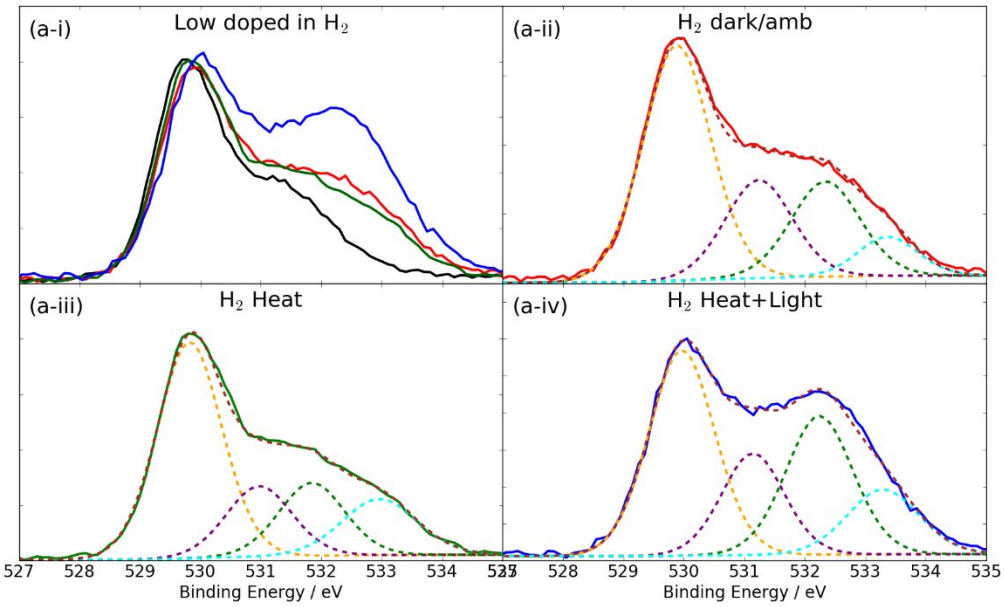

Figure S3. (a-i) The low doped sample in H_2 under the various reactor conditions and the deconvolution. (a-ii) shows the O1s spectrum in H_2 dark ambient temperature. (a-iii) shows the O1s spectrum in H_2 dark 150°C. (a-iv) shows the O1s spectrum in H_2 photo-illumination 150°C.

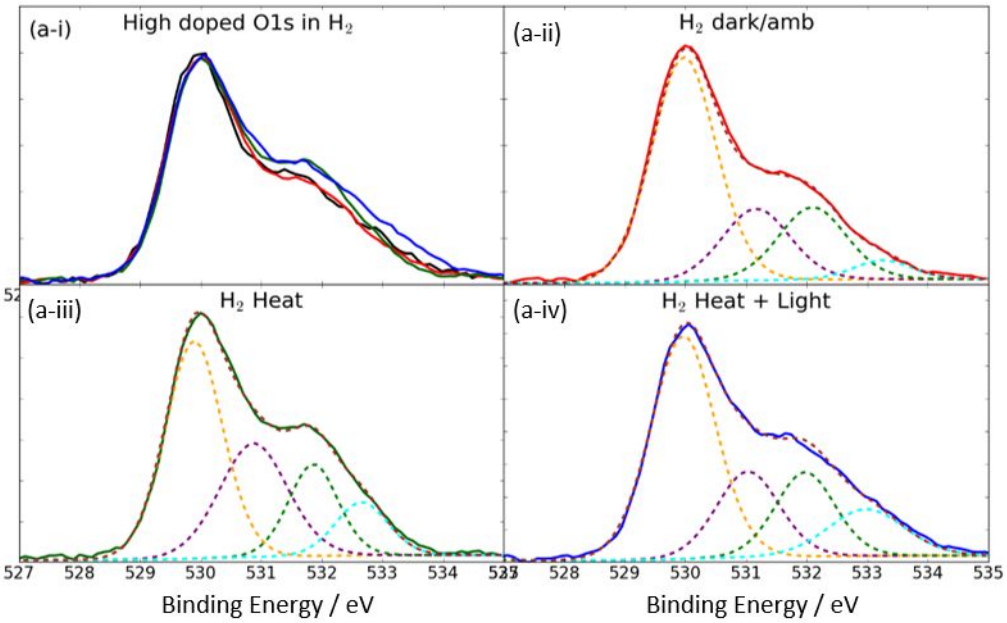

Figure S4. (a-i) The high doped sample in H_2 under the various reactor conditions and the deconvolution. (a-ii) shows the O1s spectrum in H_2 dark ambient temperature. (a-iii) shows the O1s spectrum in H_2 dark 150°C. (a-iv) shows the O1s spectrum in H_2 photo-illumination 150°C.

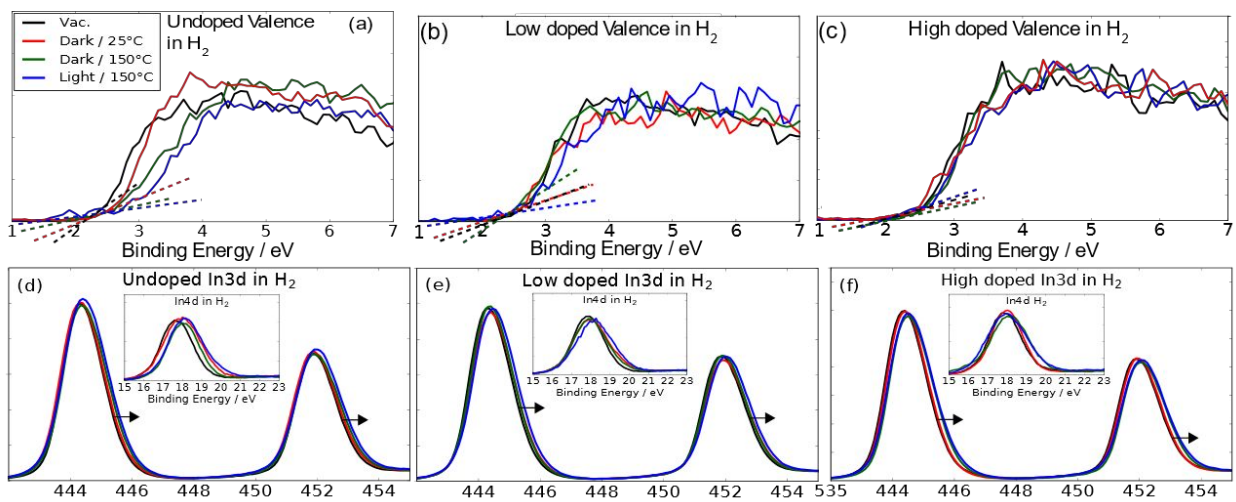

Figure S5. Valence band edge at low binding energies for samples under various reactor conditions post H_2 treatment, for undoped (a), low doped (b), and high doped (c). In3d and In4d (inset) for samples under various reactor conditions, for undoped (d), low doped (e), high doped (f) samples.

Table S1. The fractional distribution between the various O species in the deconvoluted spectra of O1s for the samples in H_2.

H_2 condition	$O_{lattice}$	O_{vac}	OH	H^+OH
Undoped Vac	0.36	0.23	0.23	0.18
Undoped dark / 30°C	0.34	0.25	0.19	0.21
Undoped dark/ 150°C	0.39	0.24	0.20	0.15
Undoped Light / 150°C	0.37	0.19	0.25	0.18
Low doped Vac	0.43	0.22	0.20	0.15
Low doped dark / 30°C	0.36	0.23	0.23	0.17
Low doped dark/ 150°C	0.36	0.21	0.21	0.20
Low doped Light / 150°C	0.33	0.21	0.26	0.19
High doped Vac	0.38	0.23	0.19	0.19
High doped dark / 30°C	0.39	0.22	0.22	0.16
High doped dark/ 150°C	0.33	0.26	0.21	0.18
High doped Light / 150°C	0.41	0.21	0.20	0.17

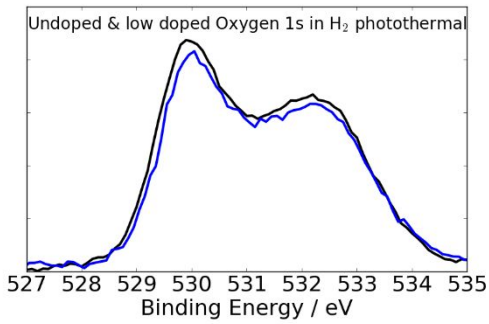

Figure S6. O1s of the undoped (black line) and low doped (blue line) sample in H_2 post photo and thermal treatment.

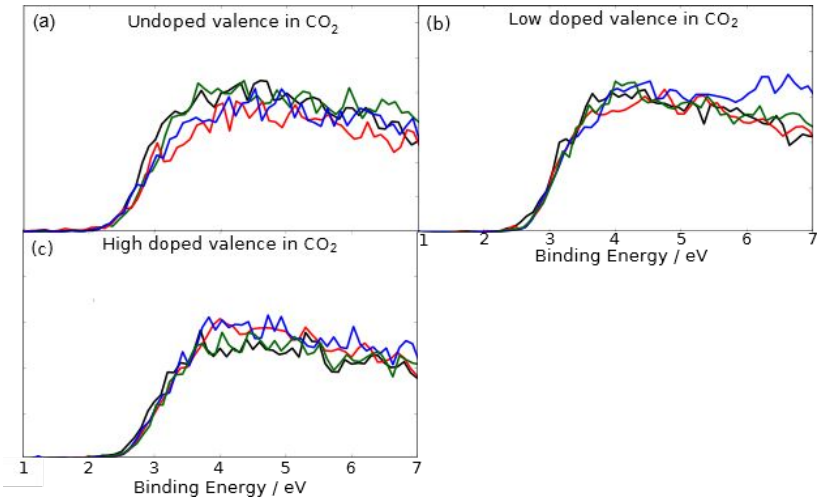

Figure S7. The valence band edge of undoped (a), low doped (b) and high doped (c) systems in CO_2 under the various reactor conditions where the black, red, green and blue lines represent vacuum, CO_2 dark ambient 25°C temperature, CO_2 dark 150°C temperature, CO_2 photo-illuminated 150°C temperature respectively.

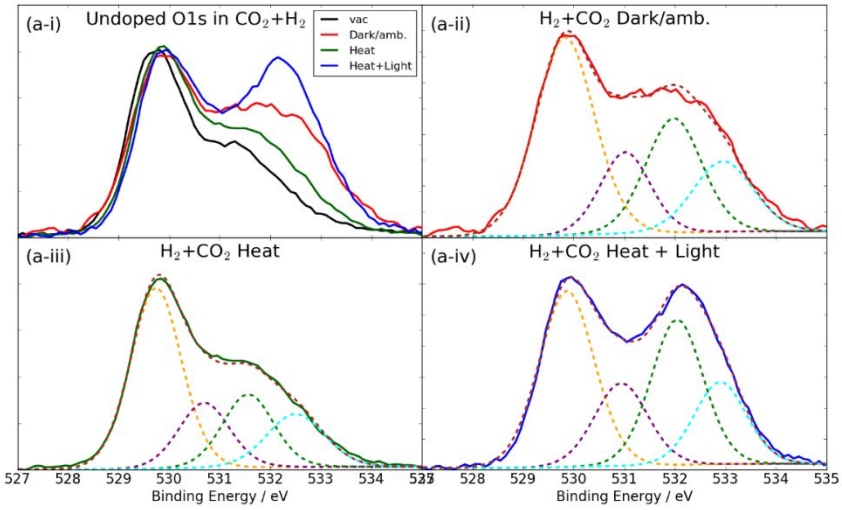

Figure S8. (a-i) The undoped sample in CO_2 + H_2 in various reactor conditions and the deconvolution. (a-ii) shows the O1s spectrum in H_2+CO_2 dark ambient temperature. (a-iii) shows the O1s spectrum in H_2+CO_2 dark 150°C. (a-iv) shows the O1s spectrum in H_2+CO_2 photo-illumination 150°C.

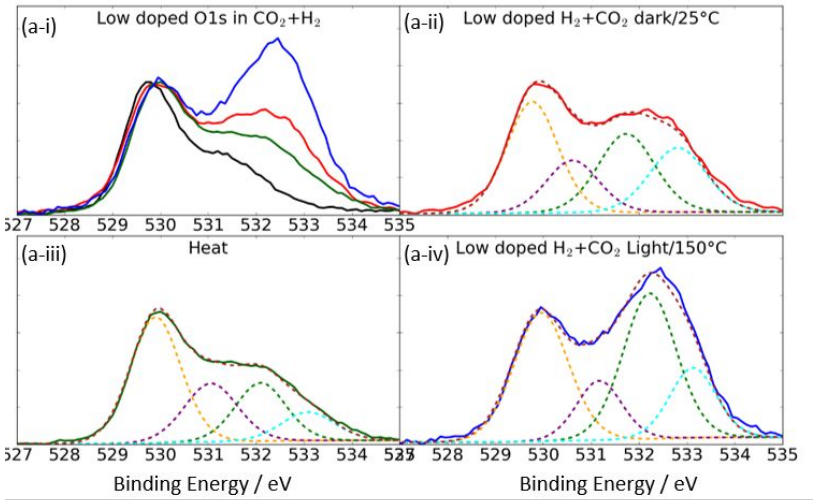

Figure S9. (a-i) The low doped sample in CO_2 + H_2 in various reactor conditions and the deconvolution. (a-ii) shows the O1s spectrum in H_2+CO_2 dark ambient temperature. (a-iii) shows the O1s spectrum in H_2+CO_2 dark 150°C. (a-iv) shows the O1s spectrum in H_2+CO_2 photo-illumination 150°C.

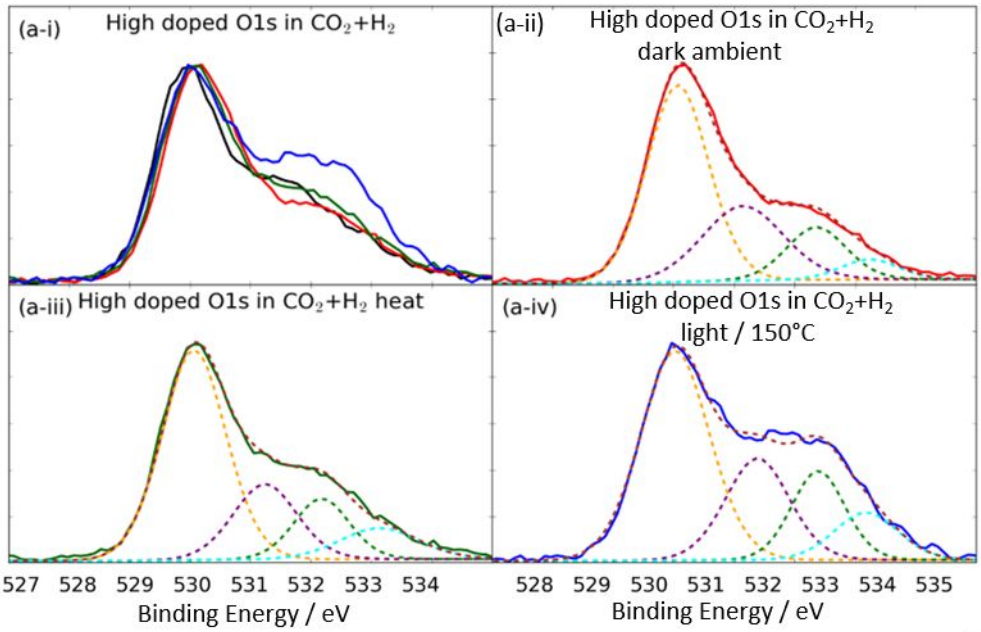

Figure S10. (a-i) The high doped sample in CO_2 + H_2 in various reactor conditions and the deconvolution. (a-ii) shows the O1s spectrum in H_2+CO_2 dark ambient temperature. (a-iii) shows the O1s spectrum in H_2+CO_2 dark 150°C. (a-iv) shows the O1s spectrum in H_2+CO_2 photo-illumination 150°C.

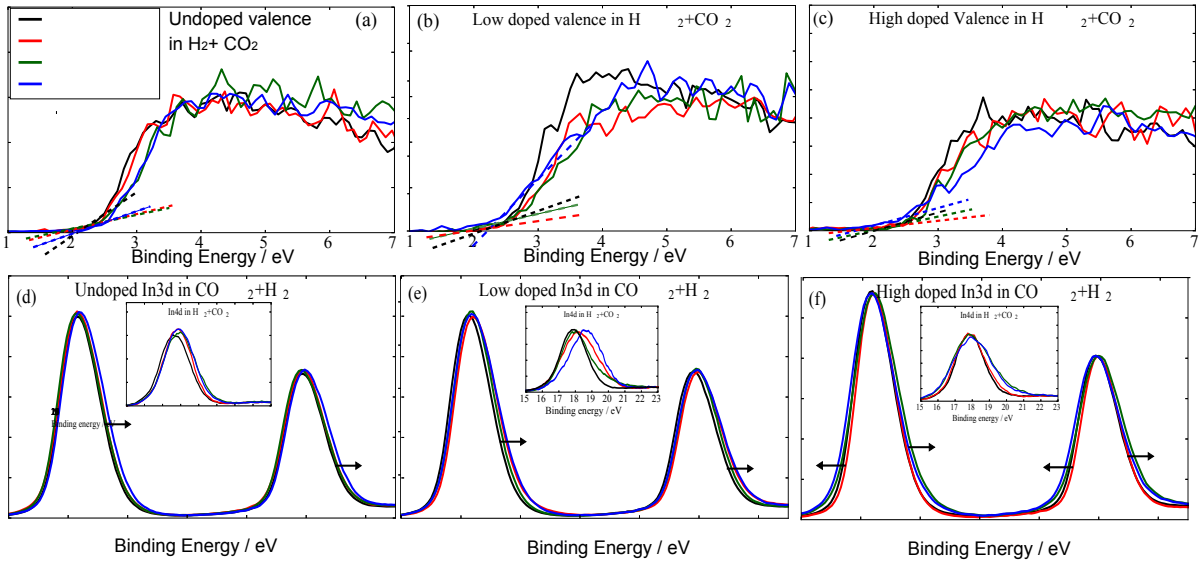

Figure S11. Valence band edge at low binding energies for samples under various reactor conditions post H_2 +CO_2 treatment for undoped (a), low doped (b), high doped (c). In3d and In4d (inset) for samples under various reactor conditions for undoped (d), low doped (e) and high doped (f).

Table S2. The fractional distribution between the various O species in the deconvoluted spectra of O1s for the samples in CO_2+H_2.

$CO_2 + H_2$ condition	$O_{lattice}$	O_{vac}	OH	H^+OH
Undoped Vac	0.36	0.23	0.23	0.18
Undoped dark / 30°C	0.37	0.19	0.25	0.19
Undoped dark/ 150°C	0.41	0.20	0.21	0.17
Undoped Light / 150°C	0.32	0.17	0.28	0.22
Low doped Vac	0.43	0.22	0.20	0.15
Low doped dark / 30°C	0.39	0.21	0.21	0.17
Low doped dark/ 150°C	0.40	0.21	0.20	0.17
Low doped Light / 150°C	0.37	0.20	0.23	0.18
High doped Vac	0.38	0.23	0.19	0.19
High doped dark / 30°C	0.45	0.20	0.16	0.17
High doped dark/ 150°C	0.40	0.21	0.16	0.17
High doped Light / 150°C	0.38	0.20	0.20	0.18

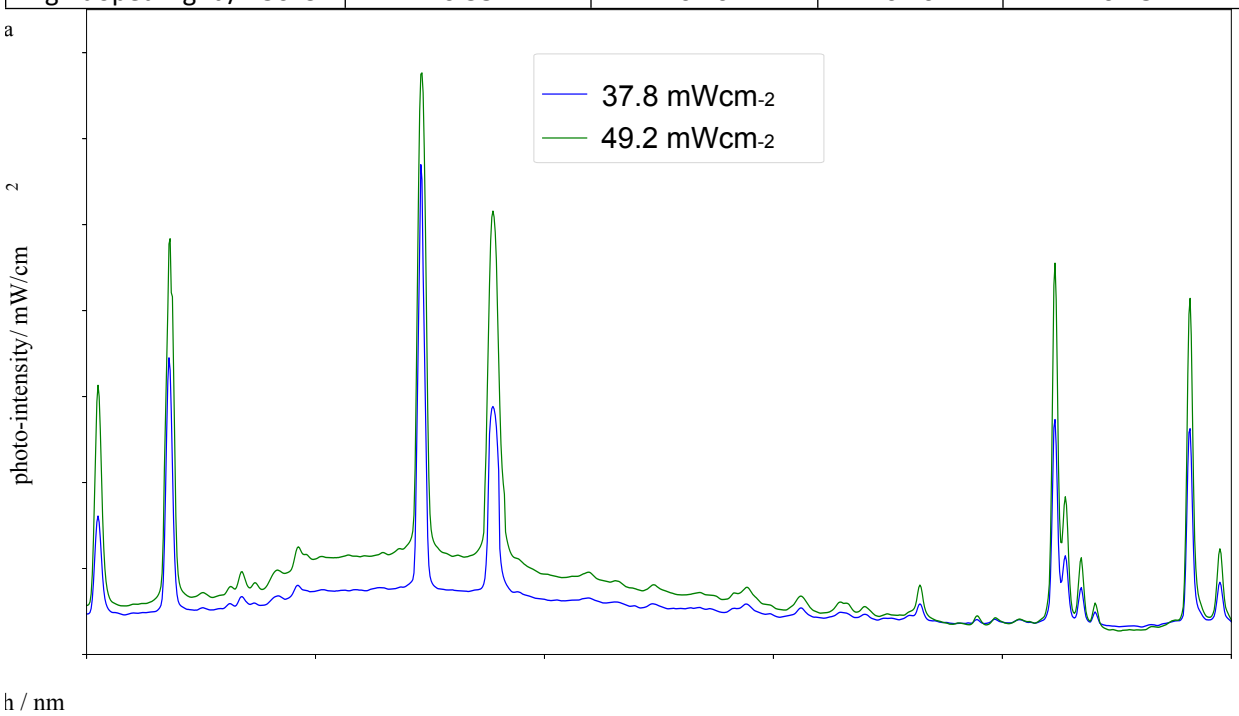

Figure S12. Optical spectroscopy of the xenon arc lamp emission at a total photo-intensity of 37.8 and 49.2 $mWcm^{-2}$. The spectrometer is a Black Comet Stellarnet™ system with 1nm resolution.

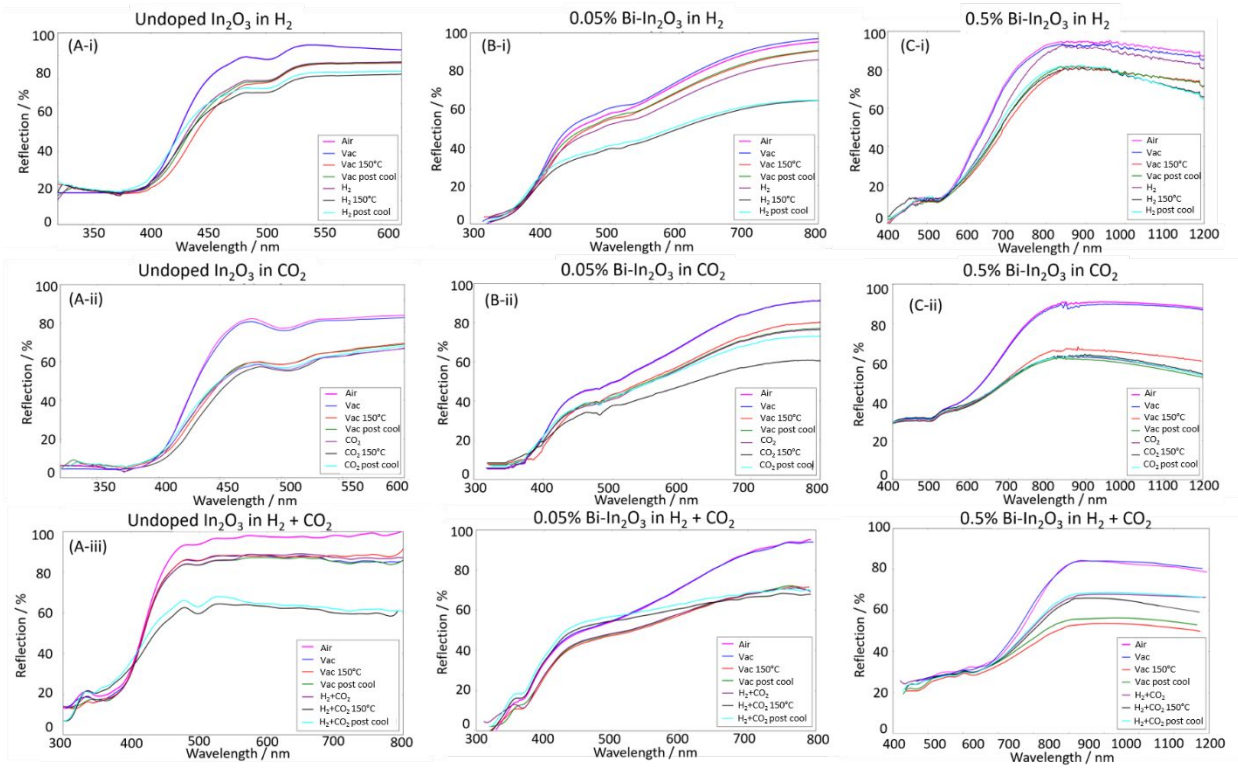

Figure S13. Raw UV Vis plots taken for various undoped and doped samples after the following sequence, air atmosphere, vacuum pump, vacuum at 150°C, vacuum cooled, gas introduction and heating of gas for 1 hour atmosphere inside modified cryostat, and post cooling.

The optical band gaps were determined from UV-Vis spectroscopy using a modified cryostat with quartz window attached to an integrating sphere for a Lambda 1100. The sample on quartz fiber paper inside the chamber situated very close to the window, was aligned with the beam slit. The cryostat was vacuum pumped before introducing H_2, CO_2 or H_2+CO_2 in a ~1:1 pressure mix. The sample was then heated for an hour before taking another spectroscopy measurement. With the results taken for the sample under vacuum, gas under ambient temperature, and gas under high temperature, a Tauc absorption algorithm was implemented to calculate the indirect band gap energy which were used to compare against the valence band edge values. The important factor is the trend in the band gap values under the gas and gas/temperature condition.

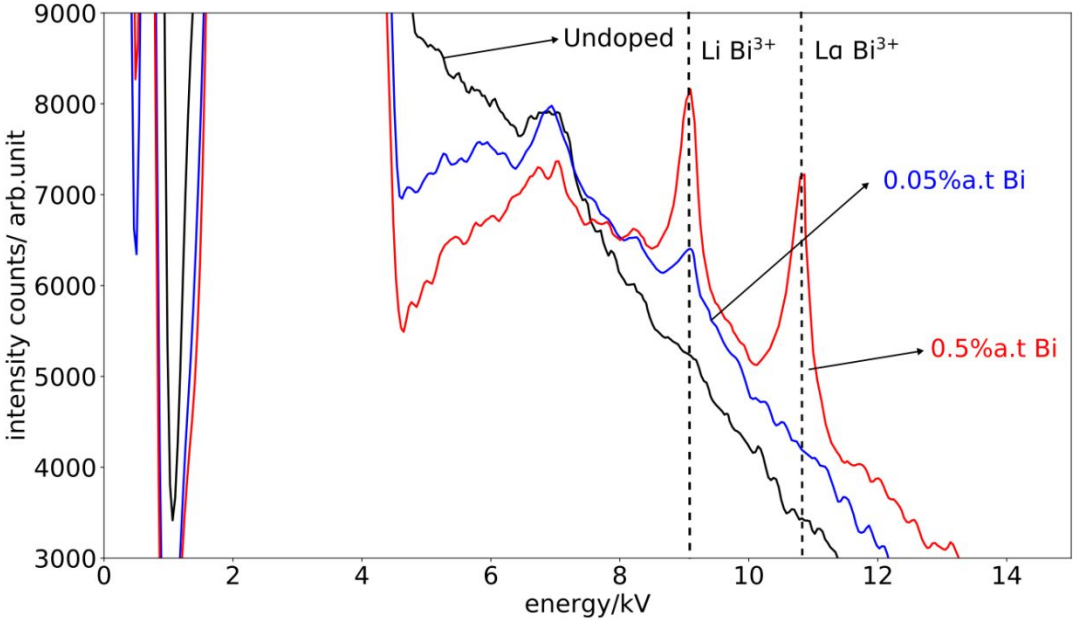

Figure S14. EDX of the various doped systems, with emphasis on the Bi^{3+} associated peaks. The Li Bi^{3+} peak at 0.5% is shown at 9.1eV for the low doped and high doped system. The area under the peak signal of the Li Bi^{3+} for 0.5% a.t Bi is 6-7 greater than the 0.05% a.t Bi.

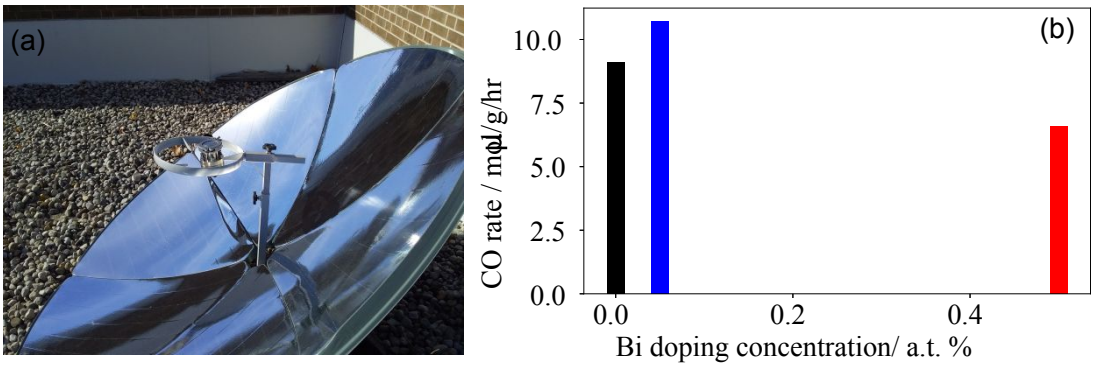

Figure S15. (a) Solar Concentrator with reactor set at the focal point of the parabolic dish. (b) CO rates as measured on concentrated photo-illuminated reactor with H2:CO2 pressure ratio of 1:1 at 32psi total pressure, on undoped (black), 0.05% a.t low doped (blue), and 0.5% a.t high doped (red) Bi_z-$In_{2-z}O_{3-x}(OH)_y$ system.

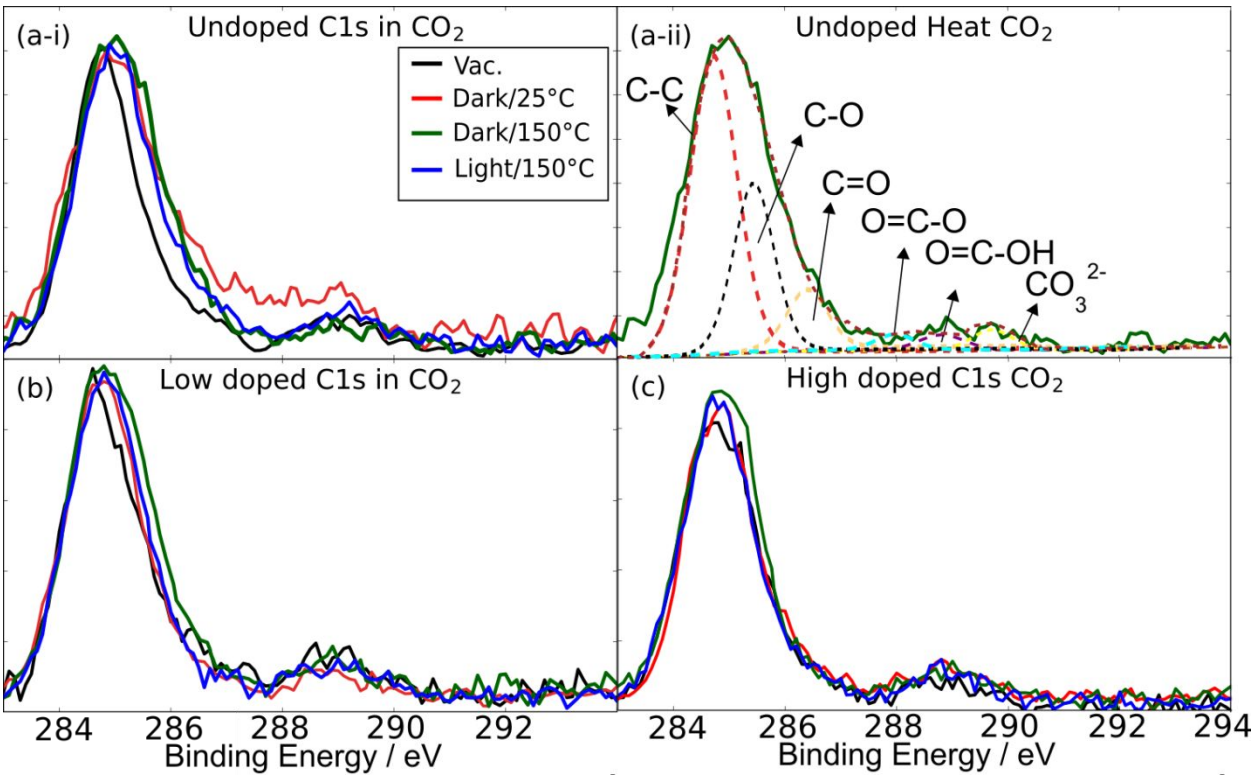

Figure S16. The C1s spectra of the various doped systems under vacuum, dark ambient temperature, dark 150°C, and photo-illumination under 150°C of CO_2 only atmosphere. (a-i) shows the undoped system. (a-ii) shows the deconvolution of the undoped C1s spectrum post dark 150°C. (b) shows the C1s of the low doped system post CO_2 reactor atmosphere. (c) shows the C1s of the high doped system post CO_2 reactor atmosphere.

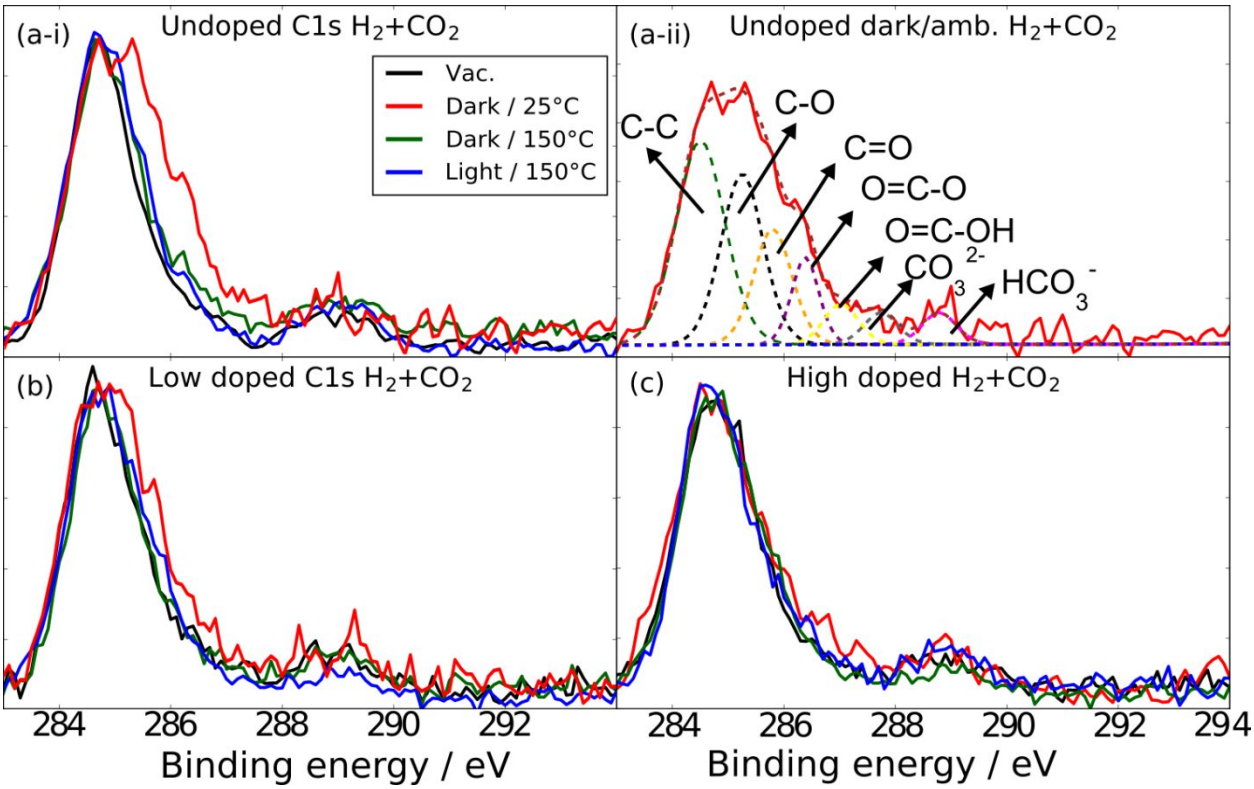

Figure S17. The C1s spectra of the various doped systems under vacuum, dark ambient temperature, dark 150°C, and photo-illumination under 150°C post CO_2+H_2 atmosphere at ~1:1 pressure ratio. (a-i) shows the undoped system. (a-ii) shows the deconvolution of the undoped C1s spectrum post dark 150°C. (b) shows the C1s of the low doped system post CO_2+H_2 reactor atmosphere. (c) shows the C1s of the high doped system post CO_2+H_2 reactor atmosphere.